Analysis of free breathing motion using artifact reduced 4D CT image data

Jan Ehrhardt[a], Rene Werner[a], Thorsten Frenzel[b], Wei Lu[c], Daniel Low[c] and Heinz Handels[a]

[a]Department of Medical Informatics,University Medical Center Hamburg-Eppendorf, 20246 Hamburg, Germany;

[b]Hermann Holthusen Institute of Radiotherapy, AK St. Georg, 20099 Hamburg, Germany;

[c]Department of Radiation Oncology, Washington University School of Medicine, St. Louis, MO 63110, USA

ABSTRACT

The mobility of lung tumors during the respiratory cycle is a source of error in radiotherapy treatment planning. Spatiotemporal CT data sets can be used for studying the motion of lung tumors and inner organs during the breathing cycle.

We present methods for the analysis of respiratory motion using 4D CT data in high temporal resolution. An optical flow based reconstruction method was used to generate artifact-reduced 4D CT data sets of lung cancer patients. The reconstructed 4D CT data sets were segmented and the respiratory motion of tumors and inner organs was analyzed.

A non-linear registration algorithm is used to calculate the velocity field between consecutive time frames of the 4D data. The resulting velocity field is used to analyze trajectories of landmarks and surface points. By this technique, the maximum displacement of any surface point is calculated, and regions with large respiratory motion are marked. To describe the tumor mobility the motion of the lung tumor center in three orthogonal directions is displayed. Estimated 3D appearance probabilities visualize the movement of the tumor during the respiratory cycle in one static image. Furthermore, correlations between trajectories of the skin surface and the trajectory of the tumor center are determined and skin regions are identified which are suitable for prediction of the internal tumor motion.

The results of the motion analysis indicate that the described methods are suitable to gain insight into the spatiotemporal behavior of anatomical and pathological structures during the respiratory cycle.

Keywords: radiation therapy, 4D CT, nonlinear registration, respiratory motion analysis

1. INTRODUCTION

Motion induced by breathing is an important uncertainty in radiotherapy planning of the thorax and upper abdomen. During treatment planning the gross tumor volume (GTV) and clinical target volume (CTV) respectively is outlined and a margin is added to account for intrafraction motion, interfraction motion, and setup error. But, in current clinical practice radiation therapy planning is often based on a static 3D CT image data set of the patient. The tumor volume and organs at risk are segmented in the static 3D CT image data. To ensure an adequate dose distribution within the moving tumor standardized safety margins are added to the tumor volume according to international guidelines.[1] However, standard safety margins usually are defined without consideration of individual motion patterns and the amount a lung tumor moves during breathing varies widely between different patients.[2] 4D CT data sets enable to measure and to visualize the individual movement of lung tumors caused by breathing and enable the patient–specific definition of safety margins. However, 4D medical image computing methods and visualization techniques are needed to extract quantitative parameters characterizing the different aspects of respiratory motion and to assist the physician in understanding the complex data.

Further author information: (Send correspondence to J.E.)
J.E.: E-mail: j.ehrhardt@uke.uni-hamburg.de, Telephone: +49 (40) 42803 9934

Furthermore, to account for respiratory motion by adding treatment margins to cover the motion of the tumor is suboptimal, because this enlarges the volume of irradiated healthy tissue and consequently, the likelihood of treatment related complications increases. Therefore, a main challenge in radiotherapy is to take breathing motion into account and to adapt the treatment according to this motion. Various techniques have been proposed to explicitly account for breathing motion during radiotherapy, like respiratory gating[3,4] or robotic radiosurgery.[5] But for implementation and optimization of these techniques a comprehensive knowledge about respiratory dynamics is needed. In particular, a reliable biometric parameter correlated with breathing motion and an accurate patient–specific spatiotemporal model of the respiratory motion is necessary to predict the target position.

4D image data with high spatial and temporal resolution acquired during free breathing enable the detailed examination of individual spatiotemporal breathing patterns. In this project, 4D CT image sequences of lung cancer patients were acquired using a multi–slice CT in cine mode during free breathing. An optical flow based temporal interpolation was used to generate artifact reduced 4D CT data sets.[6] The reconstructed 4D CT images are used for respiratory motion analysis and visualization. We present fully automated algorithms to estimate organ motion and methods to extract quantitative parameters characterizing tumor and organ motion during free breathing. Furthermore, different visualization techniques are used to present the extracted parameters.

2. MATERIAL AND METHODS

2.1. Image Acquisition and Image Reconstruction

In our approach, eight lung cancer patients were examined with a 16-slice CT scanner operated in cine-mode for the investigation of lung tumor mobility. During the acquisition process the patients were instructed to breathe naturally. The scanning of patients 1 to 4 was based on following protocol: The scanner was operated in 12-slice-mode. The scanning spatial resolution was between 0.78 x 0.78 x 1.5 mm and 0.94 x 0.94 x 1.5 mm. 16 to 19 couch positions were investigated to ensure adequate coverage of the thorax. For each couch position 15 scans were acquired continuously. Synchronized spirometry measurements were acquired to associate the CT scans with tidal volumes and breathing phase (inhalation or exhalation). The protocol for scanning patients 5 to 8 were modified slightly: The patients were scanned using 16-slice mode and acquiring 25 scans for each couch position. The scanning spatial resolution was chosen to be 0.98 x 0.98 x 1.5 mm. For further data acquisition details see Low et al.(2003)[7] and Lu et al.(2005).[8]

The resulting spatiotemporal series of CT scans were used to reconstruct 4D CT data sets. A reconstructed 4D CT image data set represents a series of 3D CT data sets for a scale of user–defined tidal volumes. Each 3D image covers the whole thorax and corresponds to a time point in the patient's breathing cycle. In the standard reconstruction approach the respiratory signal (i.e. spirometry record) is used to sort the acquired CT scans into predefined respiratory phases based on the amplitude of the respiratory trace.[8] However, free breathing causes the problem that there are no acquired CT scans for exactly the user–defined tidal volume. Therefore, data segments according to neighboring couch positions in the reconstructed 3D image represent different tidal volumes and this induces artifacts in the reconstructed image similar to motion artifacts in 3D CT. To reduce artifacts which were caused by choosing CT scans not exactly at the desired tidal volume an optical flow based reconstruction method for 4D data sets was developed.[6,9] The idea of the method is to generate interpolated CT scans for exactly the user-defined tidal volume. Therefore, a temporal interpolation scheme was derived from the optical flow equation.[10] The method to reconstruct a 3D data set for a selected tidal volume consists of two main steps: First, for each couch position the optical flow is determined between the two scans whose tidal volumes neighbor the desired tidal volume and whose breathing direction is the same as the desired direction (inhalation or exhalation). An optical flow based registration algorithm computes a velocity field describing the motion of corresponding features. The calculated velocity field is then used to generate an interpolated CT scan for the desired tidal volume. The interpolated data segments for each couch position are assembled to a 3D data set for the selected tidal volume. Due to the different number of scans per couch position the reconstructed 4D CT data sets consist of 10 3D images (patient 1 to 4) and 14 3D images (patient 5 to 8), respectively.

2.2. Modeling Respiratory Motion using Nonlinear Registration

The resulting 4D CT data sets were used to model and analyze the patient-related respiratory motion. Motion is commonly described by a displacement vector field which links the location of each point in the current volumetric frame to its location in the following frame. A large variety of automated algorithms exists to estimate organ motion, including landmark–based methods,[11,12] surface–based techniques,[13,14] optical flow based methods[15–19] and other intensity–based registration techniques, like block matching methods[20,21] or B-spline deformations.[22,23]

In this study, an optical flow based nonlinear registration method is used to estimate the trajectory of every point over the whole breathing cycle. The initial hypothesis of optical flow based methods is that pixel intensities of time varying image regions remain constant. In our case, the 4D image intensity function $I : \mathbb{R}^3 \times \mathbb{R} \to \mathbb{R}$ depends on the (time–dependent) spatial coordinate $\boldsymbol{x} \in \mathbb{R}^3$ and the tidal volume $V \in \mathbb{R}$: $I(\boldsymbol{x}(V), V)$. The conservation of the intensity of points under motion is formulated in the expression that the total derivative of the image intensity function is zero and thus, the measurement of image derivatives allows the recovery of image velocity:[15]

$$\boldsymbol{v} = -\nabla I \frac{\partial_V I}{\|\nabla I\|^2}, \tag{1}$$

where $\boldsymbol{v} = (\frac{\partial x}{\partial V}, \frac{\partial y}{\partial V}, \frac{\partial z}{\partial V})^T$ is the velocity field, ∇I the spatial image gradient and $\partial_V I$ the temporal image gradient. However, equation (1) is ill-posed and not sufficient to compute all components of the velocity vector.[15,16] Only the motion component in the direction of the local brightness gradient of the image intensity function may be estimated. As a consequence, the flow velocity cannot be computed locally without introducing additional constrains. Furthermore, the optical flow equation (1) is only valid for "small" displacements and therefore an iterative update scheme is preferable.

In our implementation an iterative solution method similar to the demon's registration[17] is used to estimate the velocity $\boldsymbol{v}_{i,j}$ between two time frames $I(\boldsymbol{x}, V_i)$ and $I(\boldsymbol{x}, V_j)$. The velocity field $\boldsymbol{v}$ describes the displacement or deformation of the image voxels and defines a transformation $\boldsymbol{\phi}$ between the two images: $\boldsymbol{\phi}(\boldsymbol{x}) = \boldsymbol{x} + \boldsymbol{v}(\boldsymbol{x})$. Thus, for a given point $\boldsymbol{x}$ in image $I(\boldsymbol{x}, V_i)$ the corresponding point $\hat{\boldsymbol{x}}$ in image $I(\boldsymbol{x}, V_j)$ is given by $\hat{\boldsymbol{x}} = \boldsymbol{\phi}_{i,j}(\boldsymbol{x})$, where the transformation $\boldsymbol{\phi}$ is defined by $\boldsymbol{\phi}_{i,j}(\boldsymbol{x}) = \boldsymbol{x} + \boldsymbol{v}_{i,j}(\boldsymbol{x})$. The necessary regularization is done using a Gaussian smoothing of this displacement field:

1. Initialize $\boldsymbol{v}^0_{i,j}(\boldsymbol{x})$, $k = 0$.
2. Estimate the update of the velocity field by

$$\boldsymbol{u}^{k+1}_{i,j}(\boldsymbol{x}) = -\nabla I(\boldsymbol{x}, V_i) \frac{\big(I(\boldsymbol{x} + \boldsymbol{v}^k_{i,j}(\boldsymbol{x}), V_j) - I(\boldsymbol{x}, V_i)\big)}{\|\nabla I(\boldsymbol{x}, V_i)\|^2 + \alpha^2 \big(I(\boldsymbol{x} - \boldsymbol{v}^k_{i,j}(\boldsymbol{x}), V_j) - I(\boldsymbol{x}, V_i)\big)^2} \tag{2}$$

3. Update the velocity field and perform a Gaussian smoothing:

$$\boldsymbol{v}^{k+1}_{ij}(\boldsymbol{x}) = G_\sigma \star \big(\boldsymbol{v}^k_{i,j}(\boldsymbol{x}) + \boldsymbol{u}^{k+1}_{i,j}(\boldsymbol{x})\big)\,. \tag{3}$$

4. Stop, if the squared distance between image $I(\boldsymbol{x}, V_i)$ and deformed image $I(\boldsymbol{x} + \boldsymbol{v}^k_{i,j}(\boldsymbol{x}), V_j)$ was not reduced for κ iterations or if a maximal number of iterations is reached. Otherwise, let $k := k + 1$ and go to 2.

The term $\alpha^2 \big(I(\boldsymbol{x} + \boldsymbol{v}^k_{ij}(\boldsymbol{x}), V_j) - I(\boldsymbol{x}, V_i)\big)^2$ in eq. (2) stabilizes the formula when the gradient norm is small and α is a homogenization factor to limit the normalized displacement in each iteration step (see Cachier et al.(1999)[24] for details). In our application we choose $\alpha = 0.5$ in order to limit the maximum displacements per iteration to the voxel-size. The standard deviation of the Gaussian kernel G_σ was set to $\sigma = 1.5$. A calculated velocity field is visualized in fig. 1.

In our application, the goal is to determine corresponding points in a sequence of images $I(\boldsymbol{x}, V_0)$, $I(\boldsymbol{x}, V_1)$, ..., $I(\boldsymbol{x}, V_{n-1})$ acquired throughout the respiratory cycle. Two approaches are possible to trace the motion of a point in a temporal image sequence:

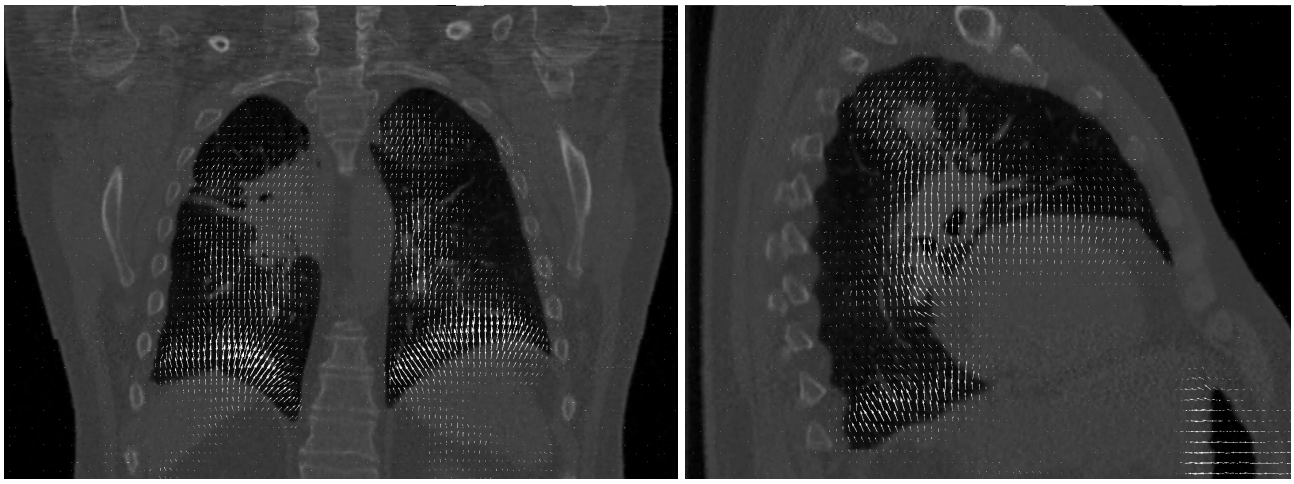

Figure 1. Visualization of the 3D motion field of the lung. Here the lung motion field of patient 5 estimated between the phase of maximum exhalation and maximum inhalation is visualized. For an improved graphical representation the motion field has been thinned out.

Registration of consecutive frames: In the first approach, adjacent images $I(\boldsymbol{x}, V_i)$ and $I(\boldsymbol{x}, V_{i+1})$ ($i = 0, \ldots, n-2$) in the temporal image sequence are registered to estimate the velocity fields $\boldsymbol{v}_{i,i+1}$. Then, starting in image $I(\boldsymbol{x}, V_0)$ the trajectory of an point $\boldsymbol{x}$ is determined by concatenating the transformations $\boldsymbol{\phi}_{0,1}$, $\boldsymbol{\phi}_{1,2}$ to $\boldsymbol{\phi}_{n-2,n-1}$ associated with the velocity fields:

$$\mathbf{X} = \begin{pmatrix} \boldsymbol{x} \\ \boldsymbol{\phi}_{0,1}(\boldsymbol{x}) \\ \boldsymbol{\phi}_{1,2} \circ \boldsymbol{\phi}_{0,1}(\boldsymbol{x}) \\ \vdots \\ \boldsymbol{\phi}_{n-2,n-1} \circ \cdots \circ \boldsymbol{\phi}_{0,1}(\boldsymbol{x}) \end{pmatrix}.$$

Because the velocity vectors are estimated for the discrete voxel lattice an interpolation is necessary. Interpolation errors are summed up and this affects the result. Otherwise, because the displacement between adjacent time frames is small an robust estimation of the velocity fields is possible. Furthermore, using this approach the regularization in eq. (2) can be done by a spatiotemporal Gaussian smoothing to limit the possible differences between magnitude and direction of spatially *and temporally* neighboring velocity vectors. The periodic nature of breathing can be addressed by implementing periodic boundary conditions for the Gaussian smoothing in time direction (see also Ehrhardt et al.(2007)[10]).

Registration with a reference frame: In this approach, the points in the sequence of images $I(\boldsymbol{x}, V_0)$, $I(\boldsymbol{x}, V_1)$, ..., $I(\boldsymbol{x}, V_{n-1})$ are mapped to the corresponding points in a reference image. The end–expiration image $I(\boldsymbol{x}, V_0)$ is used as the reference image for all registrations, since recent studies indicate that the end–expiration is in generally the most reproducible phase in the breathing cycle.[25] By successive application of the registration algorithm the vector fields $\boldsymbol{v}_{0,1}$ through $\boldsymbol{v}_{0,n-1}$ are computed that map $I(\boldsymbol{x}, V_1)$ through $I(\boldsymbol{x}, V_n - 1)$ to the reference image $I(\boldsymbol{x}, V_0)$. The trajectory of an point $\boldsymbol{x}$ in image $I(\boldsymbol{x}, V_0)$ is calculated by applying the transformations $\boldsymbol{\phi}_{0,i}$ and no concatenation of transformations is necessary:

$$\mathbf{X} = \begin{pmatrix} \boldsymbol{x} \\ \boldsymbol{\phi}_{0,1}(\boldsymbol{x}) \\ \boldsymbol{\phi}_{0,2}(\boldsymbol{x}) \\ \vdots \\ \boldsymbol{\phi}_{0,n-1}(\boldsymbol{x}) \end{pmatrix}.$$

However, using this approach a regularization of the registration process in temporal direction is harder to realize. Furthermore, large displacements are possible between distant frames which could not easily be captured by the registration process. Tissue motion during the respiratory cycle is assumed to be a smoothly continuous process and the difference between consecutive deformation fields $\boldsymbol{v}_{0,i}$ and $\boldsymbol{v}_{0,i+1}$ is expected to be relatively small. Therefore, the velocity field $\boldsymbol{v}_{0,i}$ which maps the reference frame to image $I(\boldsymbol{x}, V_i)$ is used as initial estimate for registering the reference frame to $I(\boldsymbol{x}, V_{i+1})$, i. e., when computing the velocity field $\boldsymbol{v}_{0,i+1}$. In this way, suitable starting values are given for the registration processes. However, the hypothesis of optical flow, the conservation of the intensity of points under motion, is rather acceptable for adjacent image frames than for temporal distant frames since e.g. the compression of the lung tissue leads to a change of intensities in the CT images throughout the respiratory cycle.

The computed volumetric motion model can be used to generate geometrical deformation models of organ surfaces. Therefore, a geometrical representation of the organ surface, e.g. a triangle mesh, is extracted from the selected reference frame. Then, each vertex of the geometric representation can be assigned a trajectory or the vertex coordinates are deformed using the deformation fields determined by the intensity–based registration processes to visualize the motion.

In this study, both approaches were used to determine trajectories of surface points on the lung and the skin. Although a comparison and a quantitative evaluation of both approaches is beyond the scope of this paper, this topic is discussed again in section 3.

2.3. Analysis of Respiratory Motion

In order to allow the analysis of respiratory motion the segmentation of structures of interest is necessary. Therefore, the tumor, the lung, the skin and the bronchial tree are segmented for any reconstructed tidal volume. For patient 1 to 4 these segmentations were performed using region growing techniques, morphological operators and interactive correction in each of the ten 3D data sets independently. To speed up the segmentation process an optical flow based interpolation technique[10] was used for patient 5 to 8. First, the structure of interest was segmented in the end–expiration image and the end–inspiration image. Then, structure preserving interpolation[10] was applied to generate initial segmentations for all remaining 3D images. Afterwards, the initial segmentations were corrected interactively by an physician. Surface models of the segmented organs were generated in order to enable the visualization of the 4D breathing motion and the individual tumor mobility.

In a first study, lung segmentation results were used to perform a fractional air content analysis.[8] To validate the quality of the reconstructed 4D CT images the air volume in the lungs was calculated for each 3D image of the image sequence. These values were correlated with the tidal volumes chosen for reconstruction of the 3D images considered. A strong correlation was seen as a prerequisite for high-quality motion analysis.

To describe the tumor mobility the tumor's center of mass was calculated for each 3D image of the image sequence. The tumor trajectory is expressed as the series of displacements of the mass center of successive time frames. This enables the quantification of the displacement in craniocaudal (CC), anteroposterior (AP) and lateral direction and the amount of the maximum displacement of the tumor. Moreover, 3D appearance probabilities of the tumor can be computed. Thus, the relative frequency of appearance of a tumor voxel in the sequence of 3D CT data sets represents an estimator of the tumor's appearance probability at the position considered. Hence, for each voxel the appearance probability of the tumor was estimated and visualized color-coded (fig. 2). Red areas represent voxels that were covered by the tumor during the whole breathing cycle. For the definition of motion-oriented, patient–specific treatment margins around the tumor all voxels with appearance probability $p \geq 0$ have to be covered by the margins.

To study thorax and lung deformations the optical flow of the segmented 4D data sets was calculated as described in section 2.2. The resulting deformation fields are used to approximate the trajectories of points on the organ surfaces. So, the maximum displacement of any surface point can be calculated and regions with large respiratory motion are identified (see fig. 4). Further on, the shape and deflection of different trajectories can be compared.

In radiotherapy of the thorax, it is difficult to observe the tumor motion directly during treatment. Therefore, in some applications motion of a surrogate structure, such as the chest wall, the abdomen or the diaphragm, is used to predict tumor position for the purpose of respiratory gating or robotic motion compensation. By identifying trajectories of the tumor's center and trajectories of surface points an analysis of the dependency between tumor motion and organ motion becomes possible. So, the relationship between the motion of the observed structure and tumor motion can be studied.

In our application, the main interest is to identify regions of the skin which are suitable for predicting tumor position. Let

$$\mathbf{Y} = \begin{pmatrix} y_{1,1} & y_{1,2} & y_{1,3} \\ \vdots & \vdots & \vdots \\ y_{n,1} & y_{n,2} & y_{n,3} \end{pmatrix}$$

be the trajectory of the tumor's center and

$$\mathbf{X} = \begin{pmatrix} x_{1,1} & x_{1,2} & x_{1,3} \\ \vdots & \vdots & \vdots \\ x_{n,1} & x_{n,2} & x_{n,3} \end{pmatrix}$$

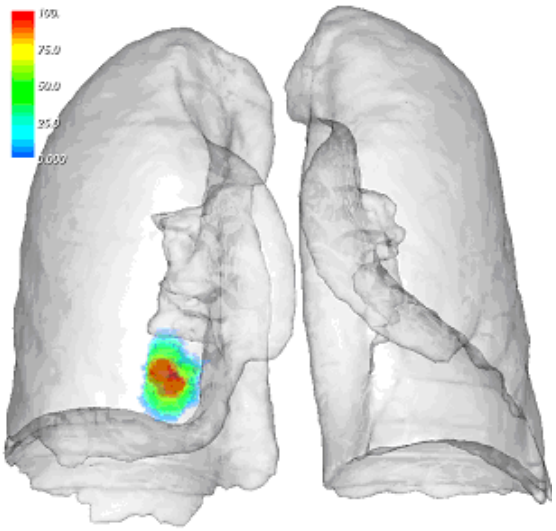

Figure 2. 3D visualization of the color-coded estimated 3D appearance probabilities of a lung tumor for patient 2. Red colored voxels belong to tumorous tissue during the whole breathing cycle. From red to blue this portion decreases.

is the trajectory of an arbitrary point. Now, a scalar measure which quantifies the dependence of the tumor motion and point motion is needed. A possible attempt is to reduce the three-dimensional motion to an one-dimensional value.[26–28] For example, the correlation between the tumor motion in CC direction and the skin motion in AP direction is considered. In order to enable a 3D–3D analysis of the relationship between tumor and skin motion a multivariate linear regression model is used. Here, a matrix $\mathbf{B}$ is sought which describes the linear dependence between the two trajectories:

$$\mathbf{Y} = \tilde{\mathbf{X}}\mathbf{B} + \boldsymbol{\mathcal{E}},$$

where $\tilde{\mathbf{X}} = (\mathbf{1}\mathbf{X})$, $\mathbf{B}$ is the matrix of regression coefficients and $\boldsymbol{\mathcal{E}}$ is the error term. The least–squares estimation of the coefficients is given by[29]

$$\hat{\mathbf{B}} = \left(\tilde{\mathbf{X}}^T\tilde{\mathbf{X}}\right)^{-1}\tilde{\mathbf{X}}^T\mathbf{Y}.$$

Now, hypothesis testing can be used to assess the significance of the predicted dependence. For instance, Wilk's Lambda for the overall regression test provides a scalar measure to rate the dependence between $\mathbf{X}$ and $\mathbf{Y}$. In our experiments, this scalar value turns out to be sensitive against noise and incorrectly determined trajectories. The frobenius norm of the residual error matrix $\|\hat{\boldsymbol{\mathcal{E}}}\|_F^2 = \|\mathbf{Y} - \tilde{\mathbf{X}}\hat{\mathbf{B}}\|_F^2$ indicates the quality of fit between the predicted trajectory $\tilde{\mathbf{X}}\hat{\mathbf{B}}$ and the true trajectory $\mathbf{Y}$. This scalar measure is more robust but is not scale invariant and thus, an inter-patient comparison is not possible. Nevertheless, the measure can be used to separate regions with high or low tumor–correlated motion.

3. RESULTS

Respiratory motion of lung, skin and tumor was analyzed in spatiotemporal CT data sets of eight lung cancer patients. The 4D CT data sets were acquired and reconstructed by the methods described in section 2.1. The optical flow based reconstruction method improves image quality of the reconstructed 4D CT data sets, significantly. The reconstructed 4D data sets consist of between 1920 (10×192 slices) and 3808 (14×272 slices) image slices with an in–plane resolution of 512×512 voxel resulting in 1–2 GB memory requirement per data set.

data set	tumor motion								tumor location
	CC		AP		LA		total		
Patient 01	5.9	mm	1.9	mm	≤ 1	mm	6.0	mm	left lung, near the heart
Patient 02	11.4	mm	3.4	mm	1.1	mm	12.0	mm	right lower lung lobe
Patient 03	2.0	mm	≤ 1	mm	≤ 1	mm	2.2	mm	right upper lung lobe
Patient 04	2.8	mm	6.0	mm	≤ 1	mm	6.7	mm	left upper lung lobe
Patient 05	4.1	mm	1.7	mm	1.1	mm	4.5	mm	left upper lung lobe
Patient 06	1.2	mm	1.2	mm	1.5	mm	2.2	mm	right upper lung lobe
Patient 07	19.6	mm	1.1	mm	2.6	mm	19.6	mm	left lingual
Patient 08	6.0	mm	≤ 1	mm	1.0	mm	6.0	mm	near right hilum

Table 1. Maximum excursion in craniocaudal (CC), anteroposterior (AP) and lateral (LA) direction of tumor mass center during breathing in 8 patient data sets with lung tumors.

Air content analysis showed excellent correlation (Pearsons correlation coefficients from 0.960 to 0.991) between calculated air content in the lungs and spirometry values for all patient data sets considered. This supports that the reconstructed 4D CT data sets are suitable for motion analysis of high accuracy.

In order to generate motion models of the reconstructed data sets both methods described in section 2.2 were applied: registration of consecutive slices and registration with a reference frame. Due to the large size of the data sets the computation of the motion models required a long time: between 25 and 40 hours per patient on a standard PC(2.2 GHz AMD Opteron, 8GB RAM). Furthermore, the main advantage of the approach by registration of consecutive slices, the possibility to regularize in temporal direction, could not be used due to run–time and memory issues. Validation of nonrigid registration algorithms is difficult and is an active area of research. Visual assessment of the registration results indicated that both registration algorithms are able to determine adequate respiratory motion and organ deformation. Our analysis methods calculate similar results basing on both registration approaches. However, small differences exist. First evaluations indicate that registration with a reference frame generates more smooth trajectories while interpolation errors introduce some noise in the trajectories calculated by registration of consecutive slices. Therefore, the following analysis results presented are based on the motion model generated by registration with a reference frame. An estimated motion field is shown in figure 1.

For a detailed analysis of the respiratory tumor motion the 3D trajectory of the tumor mass center was analyzed in different directions. The projections of the 3D trajectory in craniocaudal (CC), anteroposterior (AP) and lateral (LA) direction were considered to quantify tumor motion and to compare the tumor motions of different patients. Analysis of tumor mobility yields that amount and direction of tumor motion differ obviously between the patients. Localization and maximum excursion of the tumors of the patients considered are listed in table 1. In fig. 3 projections of the tumor trajectories in CC, AP and LA directions are presented for patient data sets 2 and 4. The tumor location in these data sets varies noticeably - patient 2: tumor in the right lower lung lobe near the diaphragm, patient 4: tumor in the upper lung lobe near the chest wall. The tumor of patient 2 moves much stronger than the tumor of patient 4 and shows a motion amplitude of more than 12 mm in predominantly craniocaudal direction. In contrast, the tumor of patient 4 moves predominantly in anteroposterior direction with a motion amplitude of about 6 mm. Thus, motion pattern of the tumor in patient 2 seems to be strongly influenced by movements of the nearby diaphragm while the motion pattern of the tumor in patient 4 seems to be influenced by movements of the chest wall. Hence, a dependency between the motion of the tumor and its location seems to be apparent.

In order to study the interrelationship among tumor motion and skin motion a multivariate regression was performed assuming a linear relationship of tumor trajectory (regressor) and skin point trajectories (regressands). In fig. 4(right) the sum of squared distances between tumor trajectory observed and tumor trajectory predicted (the frobenius norm of the residual error matrix) is shown for two patients. Furthermore, the magnitude of the displacement of skin surfaces is visualized color–coded in fig. 4(left). Thus, regions with large respiratory motion can be identified. Regarding fig. 4, for patient 7 only small displacements appear in the chest region and very large displacements appear in the abdomen. In contrast patient 2 has large displacements in the chest region.

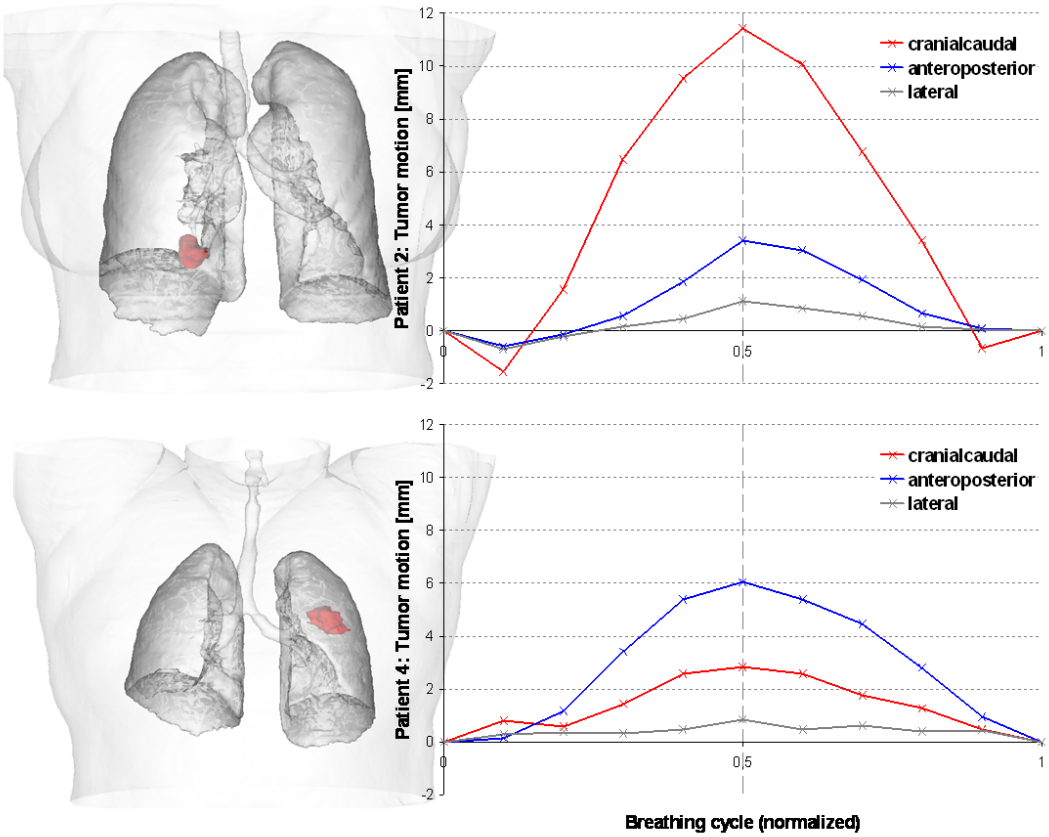

Figure 3. Left: Visualization of tumor position inside the lung for patient 2 (top) and patient 4 (bottom). Right: Motion of the tumor mass center in two patient data sets in craniocaudal, anteroposterior and lateral direction from end-inspiration (abscissa value = 0) to end-expiration (abscissa value = 0.5) and back (abscissa value = 1).

The regions of large motion agree widely with regions of a small frobenius norm of the residual error matrix. The analysis of the interrelationship among tumor motion and skin motion mainly mirrors following results: Regions on the skin which are suitable to predict tumor motion differ between the patients. Thereby, it can be stated that large motion of the skin points poses a prerequisite for tumor motion prediction. Thus, areas which were identified as suitable for tumor motion prediction widely agree with skin regions of large motion. These results indicate that the optimal position of skin markers differ from patient to patient. But further research on this topic is necessary.

4. CONCLUSION

The spatiotemporal analysis of breathing motion in 4D image data is a challenging task that opens up the possibility to get a deeper understanding of respiratory tumor and organ motion. Moreover, the analysis of individual breathing patterns is a key problem for the improvement of radiation therapy of thoracic tumors.

Reconstructed 4D image data sets were used to model respiratory motion and to analyze the motion of lung tumors and organ surface during the breathing cycle. We presented methods to calculate dense volumetric motion models and to use these models to study trajectories of organ surfaces or landmarks. Furthermore, techniques to analyze and visualize the patient–specific tumor motion and the correlation between the motion of tumor and skin were presented.

First results indicate that the tumor motion changes from patient to patient depending on the localization of the tumors in the lung and the individual differences in breathing patterns. Furthermore, first steps were done to investigate correlations between the respiratory state and the motion of skin markers in order to predict the abdominal organ motion from external, non-invasive tracking data. In contrast to other approaches like computing correlation coefficients with respect to 1D signals (point excursions, displacements in AP, RL, CC direction, etc.; e.g.[27]) methods of multivariate statistics were used to study the 3D–3D interrelationship between tumor and skin motion. Thus, thought is given to the nature of breathing caused motion of thoracic structures which generally occurs in all three spatial dimensions.

In further research the number of patient data sets will be increased and it will be of interest to analyze the breathing behavior of different patients in more detail in order to identify typical breathing patterns. The segmentation of 4D CT data consisting of up to 14 3D data sets is a time-consuming task and an automation of this process is needed. Therefore, future work will include the development of improved data driven segmentation techniques to reduce the segmentation time. Furthermore, an quantitative evaluation of the calculated motion models is necessary. Here, methods will be developed to compare different approaches for the calculation of trajectories and to quantify the precision of estimated trajectories.

REFERENCES

1. ICRU, "Report 62: Prescribing, recording and reporting photon beam therapy (supplement to ICRU report 50)," tech. rep., International Commision on Radiation Units and Measurements, 1999.
2. P. J. Keall, G. Mageras, J. M. Balter, *et al.*, "The management of respiratory motion in radiation oncology report of AAPM task group 76," *Medical physics* **33**(10), pp. 3874–3900, 2006.
3. H. D. Kubo, P. M. Len, S. Minohara, and H. Mostafavi, "Breathing-synchronized radiotherapy program at the university of california davis cancer center," *Med. Phys.* **27**(2), pp. 346–353, 2000.
4. G.-S. Mageras, E. Yorke, K. Rosenzweig, L. Braban, E. Keatley, E. Ford, S.-A. Leibel, and C.-C. Ling, "Fluoroscopic evaluation of diaphragmatic motion reduction with a respiratory gated radiotherapy system," *J Appl Clin Med Phys* **2**(4), pp. 191–200, 2001.
5. A. Schweikard, G. Glosser, M. Bodduluri, M. J. Murphy, and J. R. Adler, "Robotic motion compensation for respiratory movement during radiosurgery," *Comput Aided Surg* **5**, pp. 263–77, 2000.
6. J. Ehrhardt, R. Werner, D. Säring, T. Frenzel, W. Lu, D. Low, and H. Handels, "An optical flow based method for improved reconstruction of 4D CT data sets acquired during free breathing," *Med Phys* **34**(2), 2007. accepted.
7. D.-A. Low, M. Nystrom, E. Kalinin, P. Parikh, J.-F. Dempsey, J.-D. Bradley, S. Mutic, S.-H. Wahab, T. Islam, G. Christensen, D.-G. Politte, and B.-R. Whiting, "A method for the reconstruction of four-dimensional synchronized CT scans acquired during free breathing," *Med. Phys.* **30**(6), pp. 1254–1263, 2003.
8. W. Lu, P. J. Parikh, I. M. El Naqa, M. M. Nystrom, J. P. Hubenschmidt, S. H. Wahab, S. Mutic, A. K. Singh, G. E. Christensen, J. D. Bradley, and D. A. Low, "Quantitation of the reconstruction quality of a four-dimensional computed tomography process for lung cancer patients," *Med. Phys.* **32**, pp. 890–901, 2005.
9. J. Ehrhardt, R. Werner, T. Frenzel, D. Säring, W. Lu, D. Low, and H. Handels, "Reconstruction of 4d-ct data sets acquired during free breathing for the analysis of respiratory motion," in *SPIE Medical Imaging 2006*, J. M. Reinhardt and P. W. Pluim, eds., **6144**, pp. 6144214–1–8, (San Diego), 2006.
10. J. Ehrhardt, D. Säring, and H. Handels, "Structure-preserving interpolation of temporal and spatial image sequences using an optical flow based method," *Methods of Information in Medicine* , 2007. accepted.
11. K. Rohr, M. Fornefett, and S. Stiehl, "Approximating thin–plate splines for elastic registration: Integration of landmark errors and orientation attributes," in *IPMI'99*, pp. 252–265, 1999.
12. A. Schweikard, H. Shiomi, and J. Adler, "Respiration tracking in radiosurgery without fiducials," *Int J Medical Robotics and Computer Assisted Surgery* **1**, pp. 19–27, 2005.
13. T. McInerney and D. Terzopoulos, "Deformable models in medical images analysis: a survey," *Med Image Anal* **1**(2), pp. 91–108, 1996.

14. M. R. Kaus, T. Netsch, S. Kabus, V. Pekar, T. McNutt, and B. Fischer, "Estimation of organ motion from 4d ct for 4d radiation therapy planning of lung cancer.," in *Medical Image Computing and Computer-Assisted Intervention – MICCAI 2004*, C. Barillot, D. R. Haynor, and P. Hellier, eds., *Lecture Notes in Computer Science* **3217**, pp. 1017–1024, 2004.
15. B. K. P. Horn and B. G. Schunck, "Determining optical flow.," *Artificial Intelligence* **17**, pp. 185–203, Aug. 1981.
16. S. S. Beauchemin and J. L. Barron, "The computation of optical flow," *ACM Computing Surveys* **27**(3), pp. 433–467, 1995.
17. J.-P. Thirion, "Image matching as a diffusion process: an analogy with maxwell's demons," *Medical Image Analysis* **2**(3), pp. 243–260, 1998.
18. T. Guerrero, G. Zhang, T.-C. Huang, and K.-P. Lin, "Intrathoracic tumour motion estimation from ct imaging using the 3d optical flow method.," *Phys Med Biol* **49**, pp. 4147–4161, Sep 2004.
19. D. Sarrut, V. Boldea, M. Ayadi, J.-N. Badel, C. Ginestet, S. Clippe, and C. Carrie, "Nonrigid registration method to assess reproducibility of breath-holding with abc in lung cancer.," *Int J Radiat Oncol Biol Phys* **61**, pp. 594–607, Feb 2005.
20. H. Hufnagel, X. Pennec, G. Malandin, H. Handels, and N. Ayache, "Non-linear 2D and 3D registration using block-matching and b-splines," in *Bildverarbeitung für die Medizin*, H. Meinzer, M. Thorn, H. Handels, A. Horsch, and T. Tolxdorff, eds., pp. 325–329, 2005.
21. L. Weruaga, J. Morales, L. Nez, and R. Verd, "Estimating volumetric motion in human thorax with parametric matching constraints.," *IEEE Trans Med Imaging* **22**, pp. 766–772, Jun 2003.
22. D. Rueckert, L. Sonoda, C. Hayes, D. Hill, M. Leach, and D. Hawkes, "Nonrigid registration using free-form deformations: application to breast MR images," *IEEE Trans Med Imaging* **18**, pp. 712–721, Aug. 1999.
23. T. Rohlfing, C. R. Maurer, W. G. O'Dell, and J. Zhong, "Modeling liver motion and deformation during the respiratory cycle using intensity-based nonrigid registration of gated MR images.," *Med Phys* **31**, pp. 427–432, Mar 2004.
24. P. Cachier, X. Pennec, and N. Ayache, "Fast non–rigid matching by gradient descent: Study and improvements of the demons algorithm," Tech. Rep. 3706, INRIA, June 1999.
25. J. M. Balter, K. L. Lam, C. J. McGinn, T. S. Lawrence, and R. K. T. Haken, "Improvement of ct-based treatment-planning models of abdominal targets using static exhale imaging," *Int J Radiat Oncol Biol Phys* **41**(4), pp. 939–943, 1998/7/1.
26. S. S. Vedam, V. R. Kini, P. J. Keall, V. Ramakrishnan, H. Mostafavi, and R. Mohan, "Quantifying the predictability of diaphragm motion during respiration with a noninvasive external marker.," *Med Phys* **30**, pp. 505–513, Apr 2003.
27. N. Koch, H. H. Liu, G. Starkschall, M. Jacobson, K. Forster, Z. Liao, R. Komaki, and C. W. Stevens, "Evaluation of internal lung motion for respiratory-gated radiotherapy using MRI: Part I–correlating internal lung motion with skin fiducial motion.," *Int J Radiat Oncol Biol Phys* **60**, pp. 1459–1472, Dec 2004.
28. G. S. Mageras, A. Pevsner, E. D. Yorke, K. E. Rosenzweig, E. C. Ford, A. Hertanto, S. M. Larson, D. M. Lovelock, Y. E. Erdi, S. A. Nehmeh, J. L. Humm, and C. C. Ling, "Measurement of lung tumor motion using respiration-correlated ct.," *Int J Radiat Oncol Biol Phys* **60**, pp. 933–941, Nov 2004.
29. L. Fahrmeier and A. Hammerle, *Multivariate statistische Verfahren*, de Gruyter, 1984.

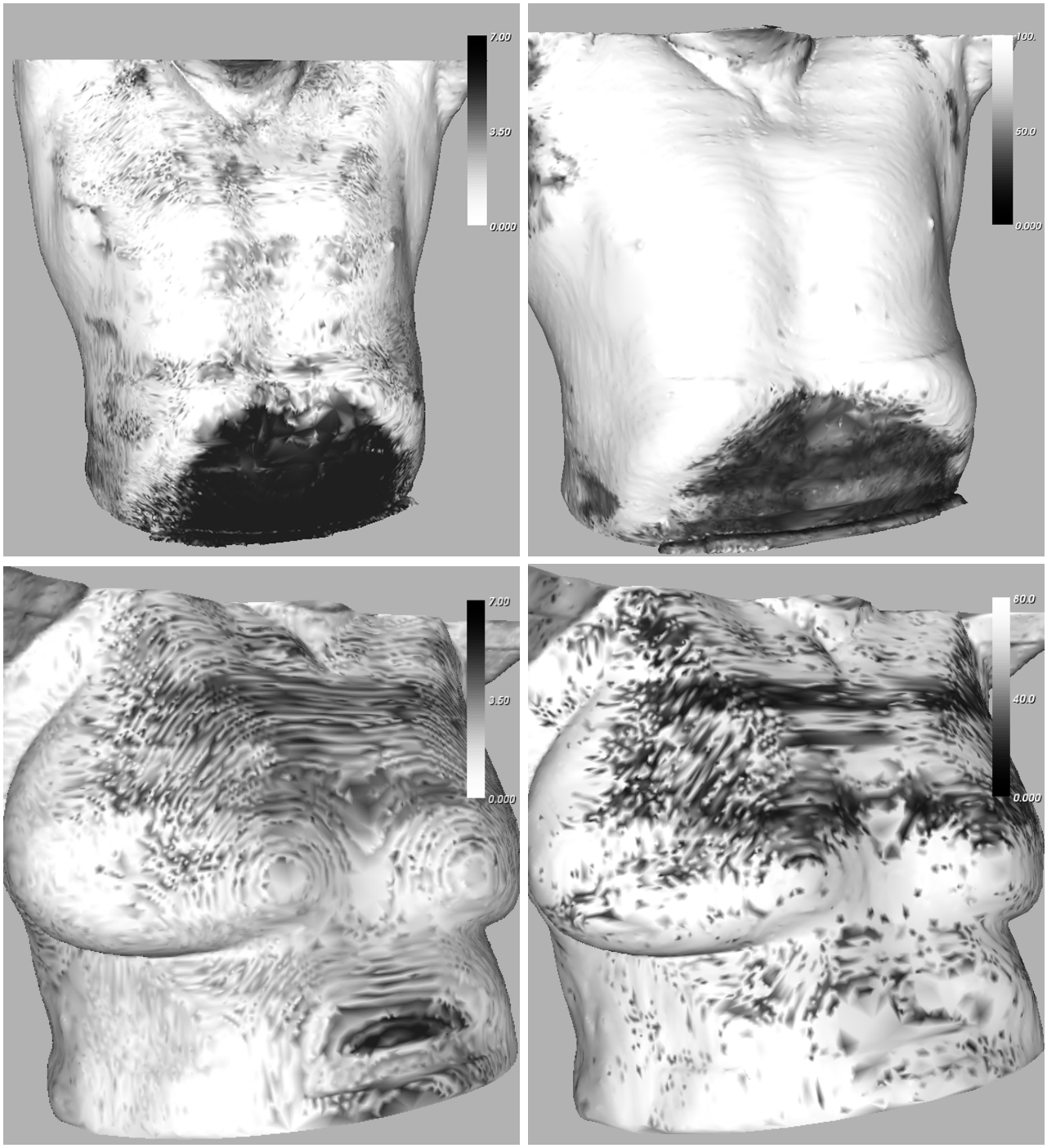

Figure 4. Left:Visualization of the maximum displacement of the skin surface during the respiratory cycle of patient 7 (top) and patient 2 (bottom). Black surface points indicate a maximum displacement $\geq 5mm$ (scale: $0 - 7$ mm) Right: Performing a multivariate regression (i.e. assuming a linear relationship) of tumor (regressor) and skin point trajectories (regressands) the SSD distance between the tumor trajectory observed and the tumor trajectory predicted is displayed.